Journal of Power Sources 244 (2013) 43–49

Contents lists available at SciVerse ScienceDirect

Journal of Power Sources

journal homepage: www.elsevier.com/locate/jpowsour

Control of interface of glass-ceramic electrolyte/liquid electrolyte for aqueous lithium batteries

Tonghuan Yang [a], Xingjiang Liu [a,b,*], Lin Sang [b], Fei Ding [b]

[a] School of Chemical Engineering and Technology, Tianjin University, Tianjin 300072, China
[b] National Key Lab of Power Source, Tianjin Institute of Power Source, Tianjin 300384, China

HIGHLIGHTS

- The water-stable lithium electrodes (WSLE) were prepared with LAGP and LATP glass-ceramic plates.
- A modified layer was deposited at glass-ceramic/organic electrolyte interface by magnetron sputtering.
- The discharge performance of WSLE was improved 70–80% by the modified layer.

ARTICLE INFO

Article history:
Received 29 November 2012
Received in revised form
15 March 2013
Accepted 13 April 2013
Available online 20 April 2013

Keywords:
Lithium-air battery
Water-stable lithium electrode
Glass-ceramic electrolyte
Interfacial modification

ABSTRACT

The discharge performance of the water-stable lithium electrode (WSLE) is improved by introducing the surface modification of the glass-ceramic plate (LAGP and LATP). The water-stable lithium electrodes are prepared with the NASICON-type glass-ceramic plates as protection layer, and using organic electrolyte as interlayer. The glass-ceramic plates with ionic conductivity of 4×10^{-4}–5.7×10^{-4} S cm^{-1} are water-stable and 300–500 μm thick. The modified layer is deposited onto the glass-ceramic plates by RF magnetron sputtering from a $Li_4Ti_5O_{12}$ target. The modified layer is analyzed by XRD, SEM-EDX, Raman and XPS. The Li-air test-cells are assembled with an SCE as reference electrode in aqueous solution. In the Li-air test-cells, the AC impedance and constant polarization potential measurements are carried out to identify the improvement of modification. The impedance of interface between the glass-ceramic plate and organic electrolyte decreases about 20–50%. Consequently, the discharge current is promoted about 70–80%. Then, by introducing interfacial modification of glass-ceramic plate, the power performance of WSLE is remarkably promoted.

1. Introduction

The lithium-air and lithium-water battery has attracted many researchers' attention, as the extremely high specific energy storage system in principle. Although the energy potentiality is high comparing with other electrochemical systems, the practical implementation still has to face several issues regarding both the electrodes and electrolytes. One of the issues, which have to be solved, is that the discharge product Li_2O_2 is insoluble in organic electrolyte and clogs the porous air-electrode gradually.

Visco et al. and Imanishi et al. proposed a water-stable lithium anode protected by $Li_3M_2(PO_4)$ solid electrolyte, which conquered this issue [1–4]. The $Li_3M_2(PO_4)$ with NASICON-type structure is a kind of water-stable lithium-ion super conductor. And since the $Li_3M_2(PO_4)$ has reduction reaction with lithium metal in contact, a lithium-ion conductive interlayer was employed between $Li_3M_2(PO_4)$ and the Li-metal. At first solid-state lithium-ion conductors have been proposed as protective interlayer, such as LiPON etc. However, the solid-state interlayer has low ionic conductivity and can't adapt to the surface-morphological changes of Li-metal electrode during discharge. Subsequently, the polymer electrolyte and organic electrolyte was proposed as the interlayer for better lithium-ion conductivity and surface-morphological adaptability [5–10]. In our previous work, it is found that the interface impedance between the solid electrolyte plate and the organic electrolyte is dominant during discharge in WSLE, which is controlling the current density [11]. Then, the interface impedance between the solid electrolyte and organic electrolyte became important. For improving the performance of water-stable lithium anode protected by solid electrolyte plate, the interface impedance must be reduced.

* Corresponding author. National Key Lab of Power Source, Tianjin Institute of Power Source, Tianjin 300384, China. Tel.: +86 (0) 22 23383783; fax: +86 (0) 22 23959300.
E-mail addresses: xjliu@nklps.org, klpsc@yahoo.com (X. Liu).

0378-7753/$ – see front matter
http://dx.doi.org/10.1016/j.jpowsour.2013.04.071

In this work, the water-stable electrolyte plates were prepared by a Li_2O–Al_2O_3–TiO_2–P_2O_5 (LATP) or Li_2O–Al_2O_3–TiO_2–P_2O_5 (LAGP) system glass-ceramic, which primarily consisted of $Li_{1+x}Ti_{2-x}Al_x(PO_4)_3$($x = 0.3$) or $Li_{1+x}Ge_{2-x}Al_x(PO_4)_3$($x = 0.5$) respectively. And the thickness was about 300–500 μm. The surface of the glass-ceramic plates was modified to promote the electrochemical performance of the interface between glass-ceramic plate and organic electrolyte.

2. Experimental

2.1. Glass-ceramic plate preparation

The LATP glass-ceramic [$14Li_2O$ $9Al_2O_3$ $38TiO_2$ $39P_2O_5$ (mol %)] exhibits high lithium-ion conductivity and has been prepared into thin plates in reports [12–14]. The $14Li_2O$ $9Al_2O_3$ $38TiO_2$ $39P_2O_5$ glass-ceramic was synthesized by reagent grade chemicals, including Li_2CO_3, Al_2O_3, TiO_2, and $NH_4H_2PO_4$. The synthesis process is same with the report by Thokchom et al. [13,14]. The LATP glass-ceramic plates were refined shape and polished to a 300–500 μm thick plate.

The LAGP glass-ceramic [$0.8Li_2O$ $0.25Al_2O_3$ $1.5GeO_2$ $1.5P_2O_5$ (mol %)] has the same structure with LATP and was made into thin electrolyte plates [15–17]. In this work, the LAGP plates were synthesized by Li_2CO_3, Al_2O_3, GeO_2, and $NH_4H_2PO_4$. The four raw materials were weighted and mixed by the stoichiometry of $0.8Li_2O$ $0.25Al_2O_3$ $1.5GeO_2$ $1.5P_2O_5$. To begin with, the mixed raw materials were heated slowly to 723 K and kept for 1.5 h to release gaseous production. Subsequently, the mixture was heated up to 1723 K and melted for 2 h. And then the molten mixture was poured in a heated plate mold and pressed by another one. The glass plate, which was casted by the molten mixture, was annealed at 823 K for 2 h and cooled in furnace. After being annealed, the glass plate crystallized at 1223 K for 12 h and became a dense opaque white specimen. This specimen was refined shape and polished to a 300–500 μm thick plate [11].

2.2. Glass-ceramic plate surface modification

A thin film of lithium titanium oxide (LTO) was deposited onto glass-ceramic plate surface by RF magnetron sputtering in argon (Ar: 50%)/oxygen (O_2: 50%) plasmas. The sputtering targets were prepared by compressing $Li_4Ti_5O_{12}$ powder (99.9%) into a 100 mm diameter pellet and were sintered at 1023 K for 6 h in air. The vacuum chamber was evacuated to a base pressure 10^{-3} Pa. The Ar/O_2 mixture gas pressure was maintained at 1 Pa. The deposition rate was 15 Å min^{-1} at 300 W RF power.

2.3. Characterizations

In all physical and electrochemical measurements, a big glass-ceramic plate was cut into 10–20 pieces of small ones (about 1 cm^2 each) in order to exclude the effect of different batches of the glass-ceramic plate. Half of them were tested after surface modification; others were tested in same way for comparison.

The surface morphology of the glass-ceramics with and without modification was characterized by a Hitachi S-4800 field emission scanning electron microscopy (SEM-EDX). The X-ray diffraction (XRD) patterns of LAGP, LATP and modified layer were recorded by a Rigaku TTRAX III diffractometer employing a Cu–Kα source. Raman spectra of samples were recorded on a Jobin-Yvon T64000 double monochromator equipped with a spatial filter. The modified layer samples, prepared for Raman testing, were deposited on nickel plate to avoid the influence of glass-ceramic plate substrate.

2.4. Electrochemical measurements

The ionic conductivity of glass-ceramic plate was measured by AC impedance. A 0.5 μm thick Ag coating was evaporated onto both sides of the glass-ceramic plate. The Ag coated plate fixed by two stainless blocking electrodes in a cell. At the room temperature (298 K), the impedance measurements were carried out on the cell using a Solartron instrument (model 1470E + 1455A) in 0.1 to 10^6 frequency range. The electrochemical impedance spectra were fitted using Zview software.

A test-cell was designed for electrochemical measurements, as shown in Fig. 1. The test-cell was separated into a Li electrode area and an air-electrode area by 0.25 cm^2 glass-ceramic plate with a thickness of 300–500 μm. The Li electrode area contained a Li-metal electrode in organic electrolyte (EC: DEC: EMC = 1: 1: 1, 1 M $LiPF_6$); the air-electrode area contained an air-electrode (Super-P carbon loaded Ni foam) and a reference electrode (an SCE connected by salt bridge) in water solution (0.5 M LiOH and 0.5 M KCl).

3. Results and discussion

Fig. 2 (LAGP) shows an XRD patterns of the LAGP plate which consists of $Li_{1+x}Al_xGe_{2-x}(PO_4)_3$($x = 0.5$) and $AlPO_4$ crystals[15–17]. The $Li_{1+x}Al_xGe_{2-x}(PO_4)_3$ ($x = 0.5$) phase is dominant in LAGP glass-ceramic, and other peaks indicate the presence of an $AlPO_4$ phase. Fig. 2 (LATP) provides an XRD patterns of the LATP plate, which consists of $Li_{1+x}Ti_{2-x}Al_x(PO_4)_3$ ($x = 0.3$) and $AlPO_4$ phases, the peaks corresponding to them are observed in XRD patterns [13,14]. The $Li_{1+x}Ti_{2-x}Al_x(PO_4)_3$ ($x = 0.3$) phase is dominant in LATP glass-ceramics. The peak around 36° indicates the presence of an $AlPO_4$ phase.

Fig. 3 shows the morphology of the LAGP surface (a, b) and LATP surface (c, d). The LAGP and LATP surface is close-grained and has visible traces of polishing. Few chips of LAGP/LATP glass-ceramic attach on surface, which were produced by polishing. Figs. 4 and 5 is the impedance spectrum of LAGP and LATP plate by blocking electrode test. The ionic conductivity of LAGP and LATP plate can be calculated and can reach 5.7×10^{-4} S cm^{-1} and 4×10^{-4} S cm^{-1}, respectively. [The formula: $\varepsilon = d/(S \cdot R)$; d: thickness of electrolyte plate; S: area of electrolyte plate; R: resistance of electrolyte plate].

Fig. 6 shows the small angle XRD patterns obtained from modified layer on LATP. The XRD pattern suggests that the LTO modified layer is amorphous, because it is prepared by RF magnetron sputtering.

Fig. 7 shows the surface morphology of the LTO modified layer on SiO_2 plate (a) and LAGP plate (b, c, d). The surface of SiO_2 is

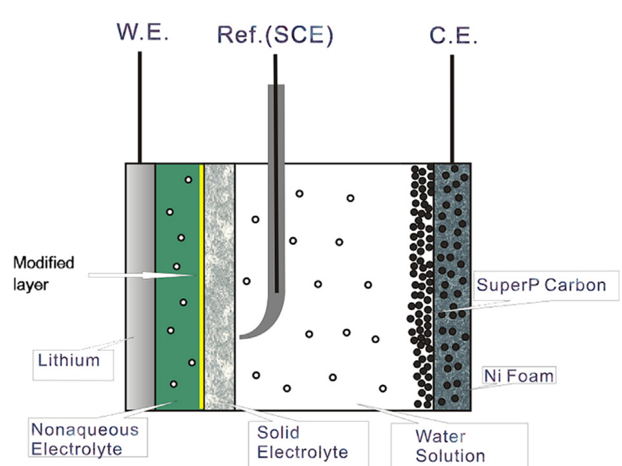

Fig. 1. A schematic representation of the 3 electrode Li-air test-cell.

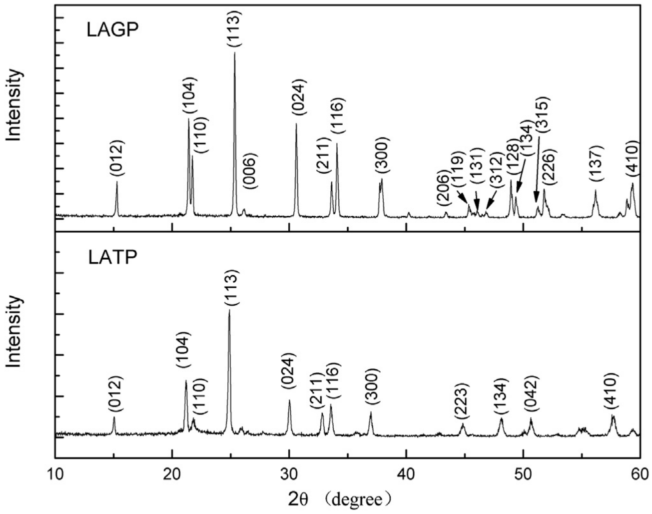

Fig. 2. XRD patterns of the LAGP and the LATP.

smoother than LAGP and LATP plate. It's better for the analysis of the LTO modified layer's morphology without the influence of morphology of the LAGP and LATP surface. As shown in Fig. 7(a), the modified layer, which is deposited onto the surface of SiO_2 substrate, is continuous and uniform. Fig. 7(b) is a SEM cross-section of a modified layer on the LAGP substrate. The cross-section shows a modified layer is deposited onto the surface of the LAGP substrate. The thickness of the modified layer is about 400 nm. Fig. 7(c, d) shows the SEM top view images of the modified layer on the LAGP surface. The modified layer is composed of many small grains and rougher than the LAGP surface. The modified layer would change the electrochemical characteristic of the interface between the organic electrolyte and LAGP plate, which covered on both hills and valleys of the whole LAGP surface. According to the observation of SEM images, the LAGP surface is completely covered by the modified layer which is prepared by RF magnetron sputtering from a $Li_4Ti_5O_{12}$ target. And the modified layer is a continuous, close-grained and uniform deposition layer, which closely growing on the LAGP surface.

Fig. 8 shows an EDX mapping of the modified layer on the LAGP for Ti element and Ge element. Existence of the Ti element of modified layer is observed and uniformly distributed. And existence of the Ge element of the LAGP substrate can also be observed, because the analysis depth of EDX is 1–2 μm which is more than the 400 nm thickness of the modified layer.

As Fig. 9(b) shows, a Raman spectrum of the $Li_4Ti_5O_{12}$ target has six characteristic bands which appear at 165, 239, 344, 430, 674, and 754 cm^{-1}. The bands at 239 cm^{-1} can be assigned to the bending vibrations of O–Ti–O bonds; the bands at 674 and 754 cm^{-1} are attributed to vibrations of Ti–O bonds in TiO_6 octahedra, the bands at 344 and 430 cm^{-1} are attributed to the stretching vibrations of the Li–O bonds in LiO_4 and LiO_6 polyhedra, respectively [18]. The weak feature at 165 cm^{-1} is attributed to bending vibrations of O–Li–O bonds and 274 cm^{-1} assigned to F2g modes [18–21].

In Fig. 9(a), the evolution of the Raman spectrum is caused by the structural changes that occurred in the LTO modified layer upon the RF magnetron sputtering. The Raman spectrum of the modified layer still has the bands at 674 and 754 cm^{-1}, which can be attributed to vibrations of Ti–O bonds in TiO_6 octahedra. The band at 430 cm^{-1} disappears due to the absent of LiO_6 polyhedra by the RF magnetron sputtering. And the Raman spectrum shows the bands at 200 and 360 cm^{-1} and the absence of the bands at 239 and 344 cm^{-1}. As Julien et al. report, the $Li_7Ti_5O_{12}$ displays a tetragonal structure with 141/amd (D_{4h}^{19}) space group, which induces three typical Raman bands located at 200, 360 and 465 cm^{-1} [21]. When $x > 1.4$ of $Li_{4+x}Ti_5O_{12}$, the Raman spectrum displays the bands at 200 and 360 cm^{-1} and the bands at 239 and 344 cm^{-1} disappear. The lack of band at 465 cm^{-1} could be attributed to the weak Raman-activity of it [21]. The band at 1096 cm^{-1} can be assigned to the vibration of CO_3^{2-} which is formed at surface in reaction between superfluous lithium and CO_2. Then, the modified layer should consist of $Li_{4+x}Ti_5O_{12}$ ($1.4 < x < 3$).

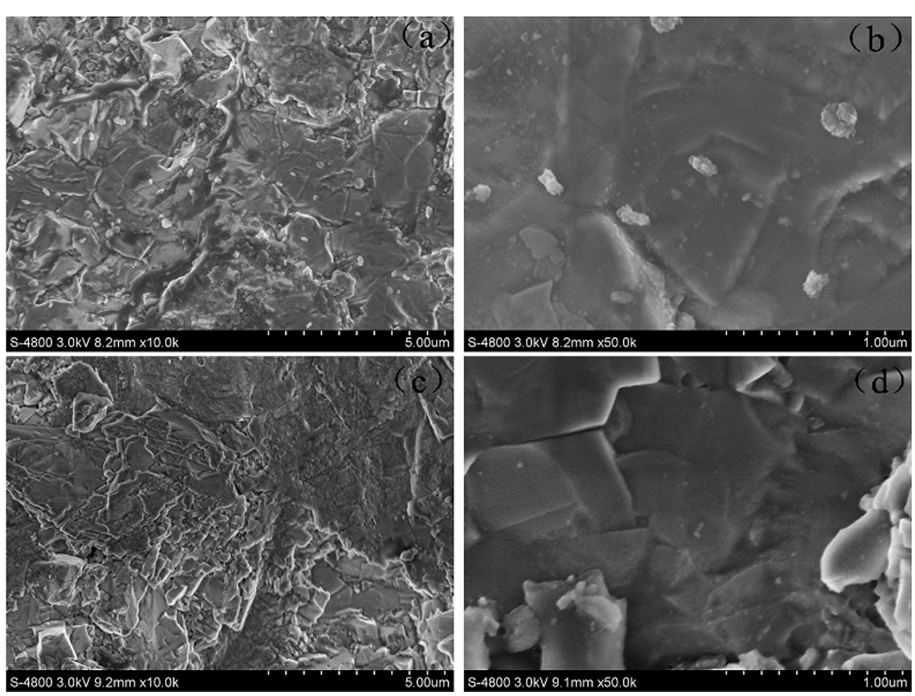

Fig. 3. SEM images of the LAGP plate (a, b) and the LATP plate(c, d).

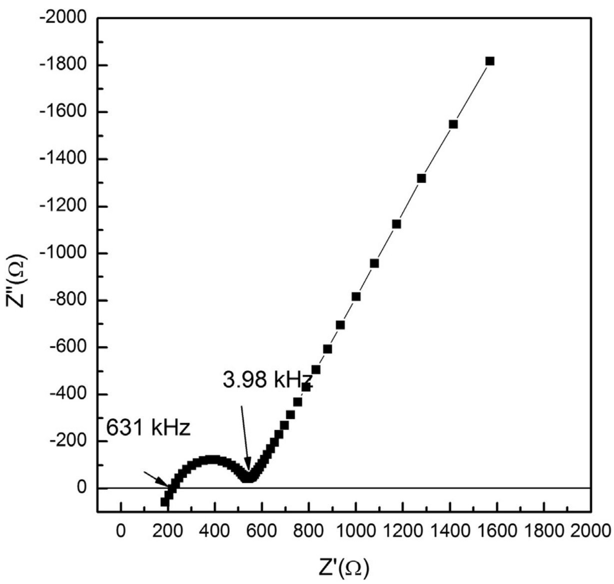

Fig. 4. Impedance spectra of the LAGP.

To obtain direct information about Ti valence of the modified layer, a modified layer is deposited onto nickel plate and studied by XPS, and the corresponding Ti 2p spectra are shown in Fig. 10. In Fig. 10, the XPS spectrum of the modified layer has two peaks at 458.8 and 464.6 eV. The two peaks of Ti 2p binding energies is mixed-valence of Ti (+IV) and Ti (+III). The binding energies at 458.8 and 464.8 eV indicate the existence of Ti (+IV) [22,23]. The peaks locate at 462.8 and 456.8 eV belongs to Ti (+III), which demonstrate the existence of Ti (+III) [22–25]. According to the analysis of each peak, the Ti (+III) occupy about 36–50%. This suggests that the x of $Li_{4+x}Ti_5O_{12}$ should be 1.8–2.5, because the x of $Li_{4+x}Ti_5O_{12}$ is equal to the number of Ti^{3+} in each five Ti-atoms. Thus, the modified layer includes Ti^{3+} and Ti^{4+}, and the x of $Li_{4+x}Ti_5O_{12}$ is 1.8–2.5, which agrees with the analysis result of Raman spectra, but more accurate.

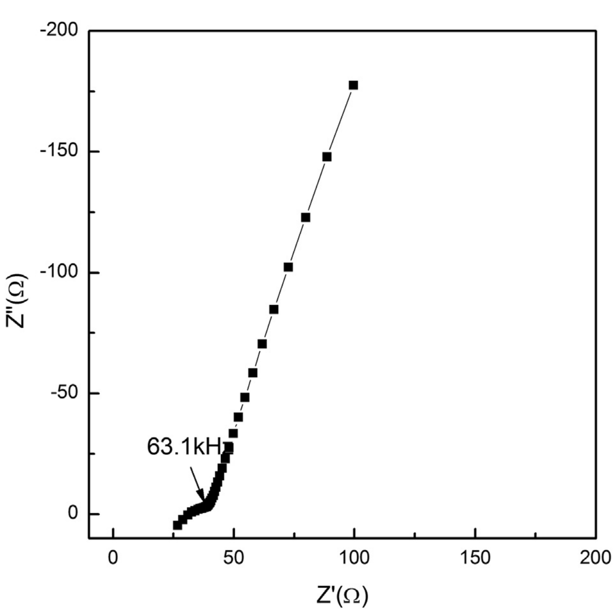

Fig. 5. Impedance spectra of the LATP.

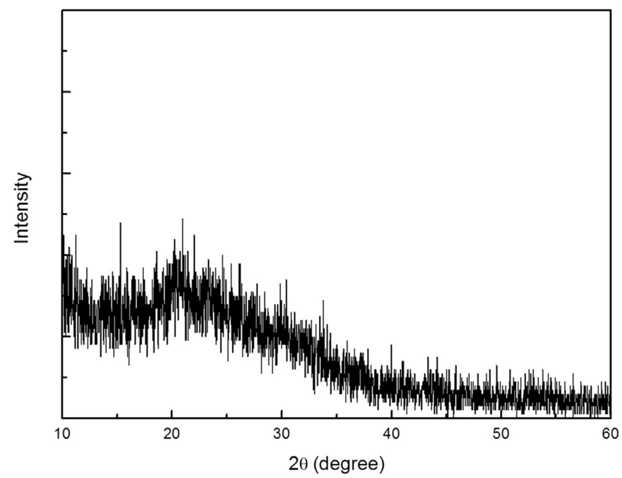

Fig. 6. XRD patterns of the LTO modified layer.

According to the analysis of EDX mapping, XRD patterns, Raman spectra and XPS spectra, the modified layer is amorphous and composed of $Li_{4+x}Ti_5O_{12}$ ($1.8 < x < 2.5$).

The water-stable lithium metal electrode consists of lithium metal, organic electrolyte, and glass-ceramics electrolyte plate, in which the organic electrolyte is employed as an interlayer to reduce the contact resistance between the glass-ceramic plate and lithium electrode, and to protect the reduction of LATP by lithium metal [2]. Fig. 11 shows impedance spectra of three-electrode test-cell with the LAGP and the modified LAGP plate. The impedance spectra of test-cell with the LAGP display a small semicircle at high frequency and a large semicircle at low frequency which may be a pressed semicircle or two overlapped semicircles. The impedance spectrum of test-cell with the modified LAGP shows a small semicircle at high frequency, a half semicircle at middle frequency and a large semicircle at low frequency. The modified layer between the LAGP plate and the organic electrolyte has made an impedance decrease of test-cell, which should be corresponding to the half semicircle at middle frequency. And the large semicircle of the LAGP test-cell should be two overlapped semicircle.

The equivalent circuit, proposed for fitting, is similar with reports, which include Re, Rg, Rint and Rsei with respective constant phase element (CPE1, CPE2 and CPE3), and W (represent a Warburg resistance) [5–7]. Re represents the bulk resistance of the LAGP plate, organic electrolyte and wires, which is corresponding to the intercept of the small semicircle with the real axis. Rg is the grain boundary resistance in LAGP plate, which is corresponding to the small semicircle. The large circle includes two overlapped semicircles, which represent the interfacial resistance of the LAGP plate at middle frequency range (Rint), and the interfacial resistance of the lithium electrode at low frequency range (Rsei). While discharging, the SEI impedance (Rsei) decreased with polarization potential, but the organic electrolyte/LAGP impedance (Rint) changed a little and became the major impedance [11]. The impedance of electrolyte/LAGP interface controlled the discharge current density [11]. Then, the improvement of modification can be estimated by the contrast of Rint, which is corresponding to the middle frequency semicircle. The simulated impedance spectra of the equivalent circuit fit with the impedance spectra well, and the parameter of the equivalent circuit is listed in Table 1.

In Table 1, Re, Rg and Rsei of the test-cell with the LAGP plate are roughly equal to the one with the modified LAGP plate. However, the Rint with modified LAGP is decreased 40%–50% (about 220 Ω). Accordingly, the discharge current of the test-cell with the modified

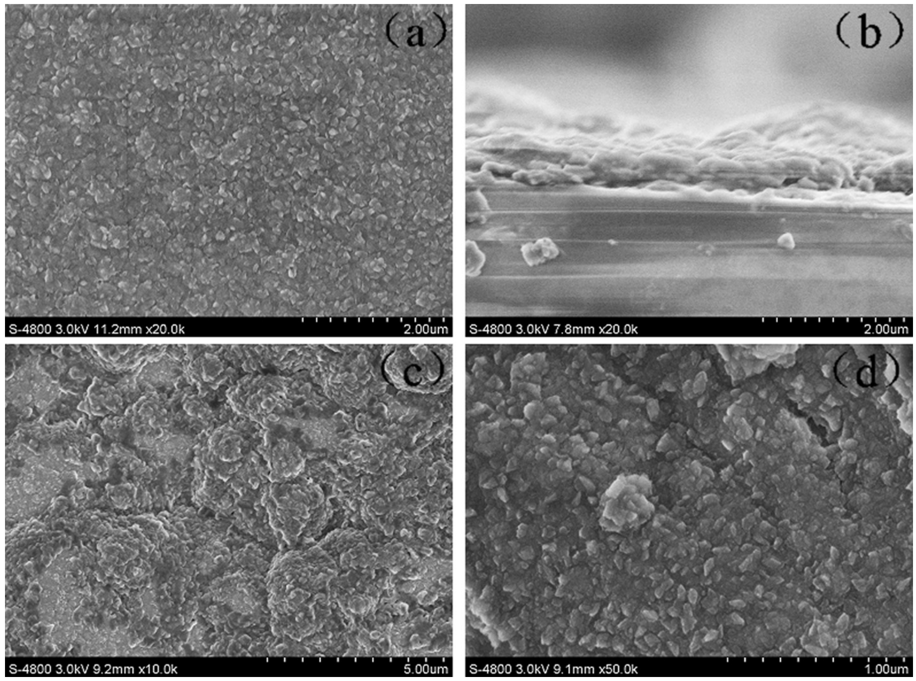

Fig. 7. SEM images of the modified layer: (a) on SiO_2; (b) a cross-section of the modified layer on the LAGP plate (c, d) on the LAGP plate.

LAGP plate should increase. Then, some tests about discharge current have been carried out.

Fig. 12 shows two constant potential polarization curves of the WSLE with and without interface modification. At −2.9 V vs. SCE (about 0.4 V vs. Li/Li^+), the current of the WSLE with interface modification is about 100% more than the one without. At the same polarization potential, the current curves of the WSLE with and without interface modification could represent the power performance when discharging. Then, the power performance of the WSLE can be remarkably promoted by introducing the modified layer, which is deposited by RF magnetron sputtering from the $Li_4Ti_5O_{12}$ target. The 50% decrease of Rint resulted in the 100% increase of discharge current, which is also an evidence of our previous results that the organic electrolyte/LAGP impedance controlled the current density when discharging [11].

At the interface of solid-state electrolyte or organic electrolyte, the ionic conduction phenomena have been explained by two different theories respectively.

At the interface of solid-state electrolyte, the phenomena are characterized by the term “nanoionics” to describe about ionic conduction [26]. At the interface, two kinds of solid-state ionic

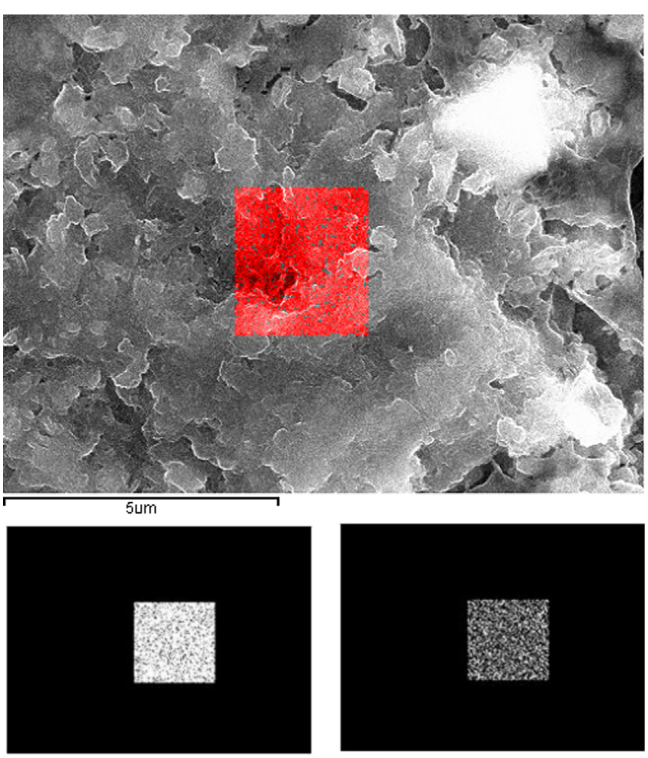

Fig. 8. EDX mapping images of the modified layer on the LAGP plate.

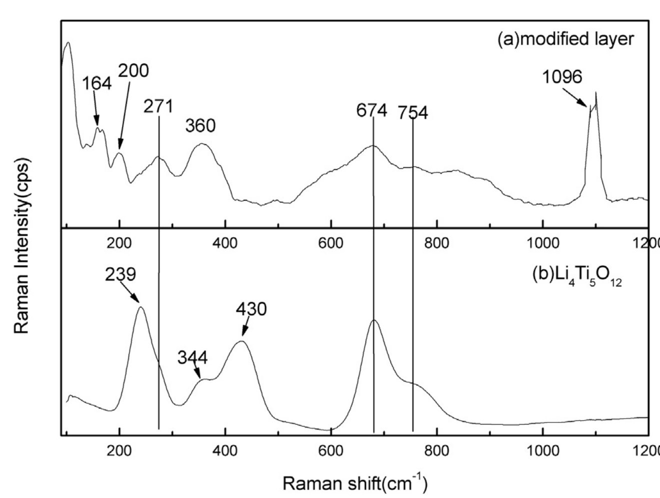

Fig. 9. Raman spectra of the LTO raw material and the LTO modified layer.

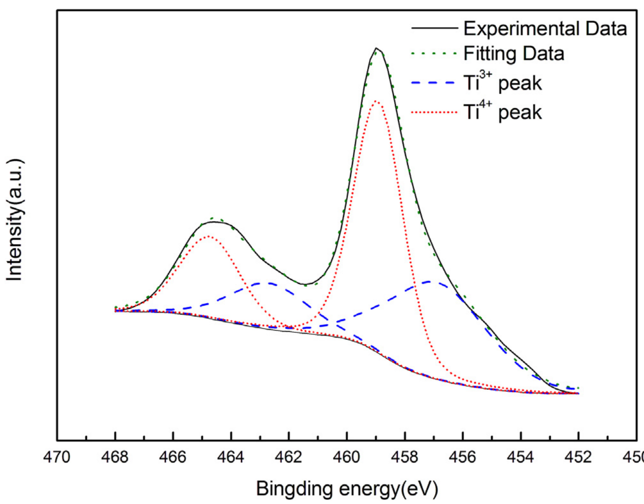

Fig. 10. XPS patterns of Ti 2p of the modified layer.

conductor correspond to two different phenomena of ionic conduction.

One is the contact of the electron-insulating ionic conductors. And one example is that two kinds of F^- ion conductor (BaF_2 and CaF_2) were brought into contact with each other [27]. The compositions and structures of solid electrolytes have been well tailored to achieve high ionic conductivities. However, the compositions deviate from the optima at the space-charge layer. And therefore, the conductivity should be lower than that of bulk, increasing the interfacial resistance [28]. For reducing the interfacial resistance, the $Li_4Ti_5O_{12}$ or $LiNbO_3$ layer is introduced as the buffer layer. Because the interposition of buffer layer can suppress the development of space-charge layer, the interfacial resistance is obviously reduced [28,29].

The other one is the contact of the mixed conductors, which are materials with a significant fraction of ionic as well as electronic. For instance, a space-charge layer in the $LiCoO_2$ should vanish when in contact with a mixed conductor, because the electronic conduction resolves the concentration gradient of the Li^+ ions [28].

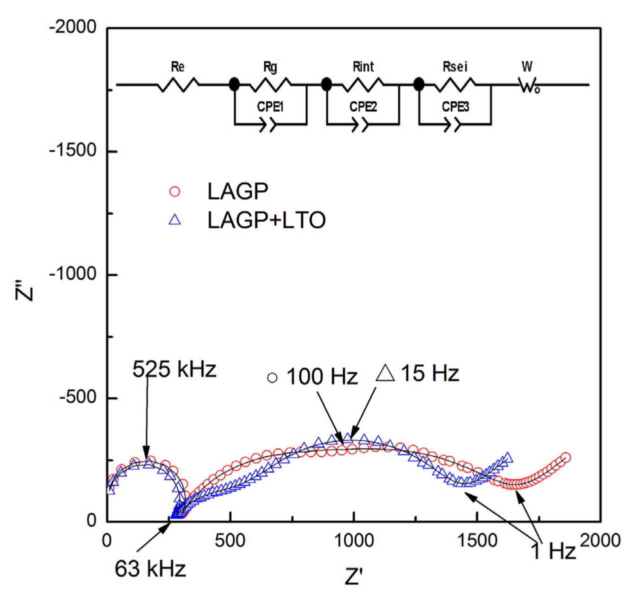

Fig. 11. Impedance spectra of the WSLE with the LAGP and the modified LAGP in the three-electrode test-cell.

Table 1
The parameter of the equivalent circuit of test-cell with LAGP and modified LAGP.

	Re (Ω)	Rg (Ω)	Rint (Ω)	Rsei (Ω)
LAGP	27	258	557	770
Modified LAGP	28	234	338	771

Similar nanoionic phenomena should take place at the LAGP side of interface between the LAGP and the organic electrolyte, developing a space-charge layer. When the LAGP is in contact with the organic electrolyte, the large difference between their chemical potentials can make Li^+ ions accumulate at LAGP interface, further developing the space-charge layer and resulting in a very large interfacial resistance. The interposition of buffer layer is a strategy which has been reported to suppress the space-charge layer [28,29]. The buffer layer introduces two interfaces: LAGP/LTO and LTO/organic electrolyte. The space-charge layers at both interfaces will be less developed, because the former consists of solid-state oxides with similar chemical potentials, and the latter consists of mixed conductor materials. And the electronic conductivity of $Li_{4+x}Ti_5O_{12}$ ($x = 1.8–2.5$) is enhanced via the generation of mixed-valence titanium [Ti (III)/Ti (IV)].

Then, the energy barrier of Li-ion transfer between the LAGP and organic electrolyte is divided into two smaller energy barriers, which are the energy barriers of LAGP/LTO interface and LTO/organic electrolyte interface. The actual process may be more complex, which needed further study.

And the $Li_{4+x}Ti_5O_{12}$ ($1.8 < x < 2.5$) should be a zero strain compound, which has the similar characteristic of $Li_4Ti_5O_{12}$ [30]. In that case, even if the formation of space-charge layer made lithium-ion unhomogeneously distribute, there still has no strain to break the modified layer.

Fig. 13 shows the impedance spectra of the three-electrode test-cell with the LATP and the modified LATP plate. The impedance spectrum of test-cell with the LATP and the modified LATP displays a small semicircle at high frequency, a half semicircle at middle frequency, and a large semicircle at low frequency which is corresponding to the SEI impedance. Same to LAGP plate, the equivalent circuit include Re, Rg, Rint and Rsei with respective constant phase elements (CPE1, CPE2 and CPE3), and W (represents a Warburg resistance). Re is corresponding to the intercept of the small semicircle with the real axis, and Rg is corresponding to the small semicircle. Rint is corresponding to the half semicircle, and Rsei is

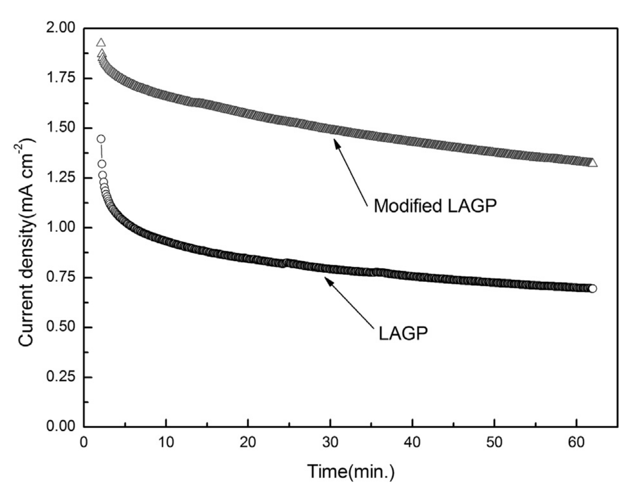

Fig. 12. Constant potential polarization curves of the WSLE with the LAGP and the modified LAGP at −2.9 V vs. SCE at 298 K.

Table 2
The parameter of the equivalent circuit of test-cell with LATP and modified LATP.

	Re (Ω)	Rg (Ω)	Rint (Ω)	Rsei (Ω)
LATP	42	194	979	1160
Modified LATP	38	205	732	1128

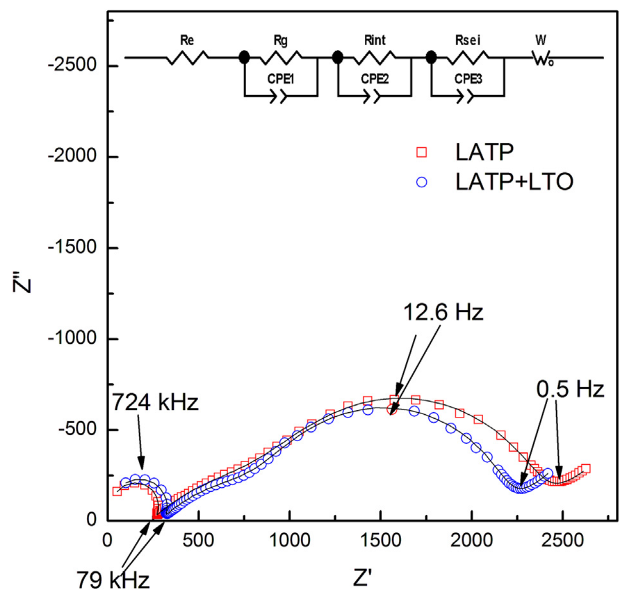

Fig. 13. Impedance spectra of the WSLE with the LATP and the modified LATP in the three-electrode test-cell.

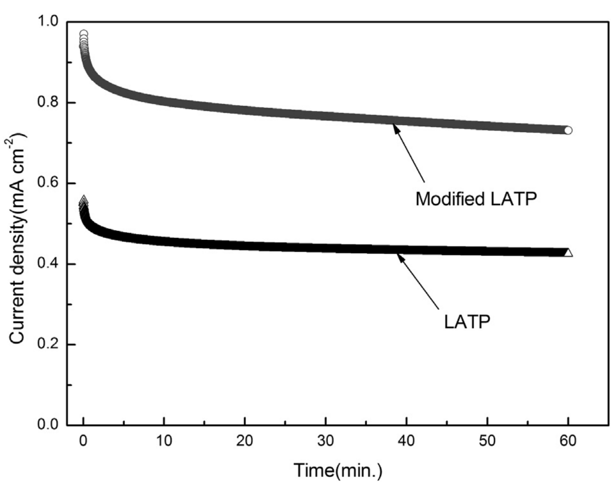

Fig. 14. Constant potential polarization curves of the WSLE with the LATP and the modified LATP at −2.9 V vs. SCE at 298 K.

corresponding to the large semicircle at the low frequency. The fitting lines of impedance spectra are also showed in Fig. 13, and the analysis results of impedance are listed in Table 2.

In Table 2, Rint with LATP is more than LAGP, which should be attributed to the low Li-ion conductivity of LATP and could also be different from actual area. Rint with modified LATP decreased about 240 Ω which is 20–30% of Rint without modification.

Fig. 14 shows two constant potential polarization curves of the WSLE protected by the LATP with and without interface modification. At −2.9 V vs. SCE (about 0.4 V vs. Li/Li^+), the current of the WSLE with interface modification is about 80% more than the one without. Then, the power performance of WSLE can be remarkably promoted by the modified layer, which is similar as the modification of LAGP plate Fig. 12.

4. Conclusion

By using the modification of the interface between the glass-ceramic (LAGP/LATP) plate and the organic electrolyte, the discharge performance of the WSLE can be remarkably promoted in aqueous solution.

The modified layer decreased the interfacial impedance between the glass-ceramic plate and organic electrolyte. The modified layer $Li_{4+x}Ti_5O_{12}$ ($1.8 < x < 2.5$) can offer more lithium-ions and vacancy sites and has electronic conduction. And, it introduced two interfaces, such as glass-ceramic plate/LTO and LTO/organic electrolyte, at which the space-charge layer was less developed. Because the $Li_{4+x}Ti_5O_{12}$ ($1.8 < x < 2.5$) the modified layer is a mixed conductor and covered the whole LAGP plate, which buffered the direct contact between the glass-ceramic plate and organic electrolyte. Then, the energy barrier of Li-ion transfer between the LAGP and organic electrolyte become two relative small energy barriers.

References

[1] S.J. Visco, E. Nimon, B. Katz, L.C.D. Jonghe, M.Y. Chu, Abstract 0389, The Electrochemical Society Meeting Abstracts vol. 2006–2, Cancun, Mexico, 2006. Oct. 29–Nov. 3.
[2] S.J. Visco, E. Nimon, B. Katz, L.C.D. Jonghe, M.Y. Chu, Abstract 53, The 12th International Meeting on Lithium Batteries Abstracts, Nara, Japan, 2004.
[3] T. Zhang, N. Imanishi, S. Hasegawa, A. Hirano, J. Xie, Y. Takeda, O. Yamamoto, N. Sammes, J. Electrochem. Soc. 155 (2008) A965.
[4] S. Hasegawa, N. Imanishi, T. Zhang, J. Xie, A. Hirano, Y. Takeda, O. Yamamoto, J. Power Sources 189 (2009) 371.
[5] T. Zhang, N. Imanishi, S. Hasegawa, A. Hirano, J. Xie, Y. Takeda, O. Yamamoto, N. Sammes, Electrochem. Solid-State Lett. 12 (2009) A132.
[6] T. Zhang, N. Imanishi, Y. Shimonishi, A. Hirano, J. Xie, Y. Takeda, O. Yamamoto, N. Sammes, J. Electrochem. Soc. 157 (2010) A214.
[7] T. Zhang, N. Imanishi, A. Hirano, Y. Takeda, O. Yamanoto, Electrochem. Solid-State Lett. 14 (2011) A45.
[8] Y. Wang, H. Zhou, J. Power Sources 195 (2010) 358.
[9] P. He, Y. Wang, H. Zhou, Electrochem. Commun. 12 (2010) 1686.
[10] P. He, Y. Wang, H. Zhou, J. Power Sources 196 (2011) 5611.
[11] T. Yang, L. Sang, F. Ding, J. Zhang, X. Liu, Electrochim. Acta. 81 (2012) 179.
[12] J. Fu, Solid State Ionics 96 (1997) 195.
[13] J.S. Thokchom, B. Kumar, Solid State Ionics 177 (2006) 727.
[14] J.S. Thokchom, B. Kumar, J. Electrochem. Soc. 154 (2007) A331.
[15] G.Y. Aleshin, D.A. Semenenko, A.I. Belova, T.K. Zakharchenko, D.M. Itkis, E.A. Goodilin, Y.D. Tretyakov, Solid State Ionics 184 (2011) 62.
[16] K. He, Y.H. Wang, C.K. Zu, Y.H. Liu, H.F. Zhao, B. Han, J. Chen, Chin. J. Inorg. Chem. 27 (2011) 2484.
[17] J. Kumar, B. Kumar, J. Power Sources 194 (2009) 1113.
[18] P.P. Posini, R. Mancini, L. Petrucci, V. Contini, P. Villano, Solid State Ionics 144 (2001) 185.
[19] C. Julien, 136-137, Solid State Ionics (2000) 887.
[20] T. Yi, L. Jiang, J. Liu, M. Ye, H. Fang, A. Zhou, J. Shu, Ionics 17 (2011) 799–802.
[21] C.M. Julien, M. Massot, K. Zaghid, J Power Sources 136 (2004) 72–79.
[22] P.W. Seo, S.S. Kim, S.C. Hong, Korean J. Chem. Eng. 27 (2010) 1220.
[23] J.Y. Luo, L.J. Chen, Y.J. Zhao, P. He, Y.Y. Xia, J. Power Sources 194 (2009) 1075.
[24] C. Trapalis, V. Kozhukharov, B. Samuneva, J. Mater. Sci. 28 (1993) 1276.
[25] R. Cai, S. Jiang, X. Yu, B. Zhao, H. Wang, Z. Shao, J. Mater. Chem. 22 (2012) 8013.
[26] J. Maier, Nat. Mater. 4 (2005) 805.
[27] N. Sata, K. Eberman, K. Eberl, J. Maier, Nature 408 (2000) 946.
[28] N. Ohta, K. Takada, L. Zhang, R. Ma, M. Osada, T. Sasaki, Adv. Mater. 18 (2006) 2226.
[29] Y. Seino, T. Ota, K. Takada, J Power Sources 196 (2011) 6488.
[30] T. Ohzuku, A. Ueda, N. Yamamoto, J. Electrochem. Soc. 142 (1995) 1431.